Leveraging the Landsat Archive to Track Understory Evergreen Shrub Expansions in the Coweeta Basin, North Carolina

Daniel James Donahoe

Thesis submitted to the faculty of the Virginia Polytechnic Institute and State University
in partial fulfillment of the requirements for the degree of

Master of Science
In
Geography

Lisa M. Kennedy, Committee Chair
Arvind A. R. Bhuta
Valerie A. Thomas

May 6, 2022
Blacksburg, Virginia

Keywords: Remote sensing, Landsat, Biogeography, Rhododendron, Mountain laurel

Leveraging the Landsat Archive to
Track Understory Evergreen Shrub Expansions
in the
Coweeta Basin, North Carolina

Daniel James Donahoe

ABSTRACT

Invasive species introductions, namely the chestnut blight fungus (*Cryphonectria parasitica*) and hemlock woolly adelgid (*Adelges tsugae*), have permanently altered the overstory canopy of Appalachian forests by causing the dramatic die-offs of two ecologically significant tree species, American chestnut (*Castanea dentata*) and eastern hemlock (*Tsuga canadensis*). These canopy dominants once had significant roles in regulating understory communities. The loss of these trees, along with fire suppression, has driven two common evergreen shrubs, rosebay rhododendron (*Rhododendron maximum*) and mountain laurel (*Kalmia latifolia*), to expand and proliferate in areas where they were once restricted. These two common shrubs are recognized agents of change in Appalachian forests because of their abilities to modify soil seed banks, regulate light, and alter the local soil chemistry. This study documented evergreen shrub expansion across the Coweeta Creek basin over the past 36 years analyzing changes in winter greenness using harmonized multi-decadal archives of Landsat imagery. We found the greatest change in winter greenness in relatively dry areas: higher elevations (1275–1300 m), steeper slopes (33°–35°), southward aspects, and far from streams (600–800 m). Historical field data collected in three unmanaged watersheds at Coweeta showed a simultaneous decrease in *T. canadensis* and increase in *R. maximum*. We also documented the decline of a xerophytic canopy tree species, pitch pine (*Pinus rigida*), and an associate understory shrub, *K. latifolia*. Our analysis of the influence of terrain variables on evergreen shrub expansion allowed us to determine which of the two species was expanding in various locations with reasonable certainty. This study provides spatially explicit data on the expansion of two evergreen shrub species at the Coweeta Hydrologic Laboratory that could be used to pinpoint areas for future management interventions.

Leveraging the Landsat Archive to
Track Understory Evergreen Shrub Expansions
in the
Coweeta Basin, North Carolina

Daniel James Donahoe

GENERAL AUDIENCE ABSTRACT

Forests in the eastern United States have changed substantially in response to the introduction of highly competitive invasive species. Some overstory tree species have been virtually eliminated from their functional role in regulating understory vegetation in many southern Appalachian ecosystems. Die-offs of these trees have allowed understory evergreen shrubs to expand into areas where they were once restricted. Shrubs that have expanded in response to overstory tree die-offs can alter the ecology of forests for the foreseeable future. Our work leveraged multi-decadal archives of wintertime satellite imagery to document the spread of understory evergreen shrubs in a watershed located in western North Carolina. We investigated the relationship of this spread to local environmental characteristics like elevation, steepness (slope), slope direction (north, south, east, west), and distance-from-stream. The greatest changes in evergreen vegetation were documented on terrain at relatively high elevations, locations farther from streams, on southerly aspects, and on relatively steep terrain. We included historical field data collected during the same time period that showed a simultaneous increase in two understory evergreen shrub species after the die-off of ecologically significant overstory tree species. This information will help forest managers by describing areas where substantial spread has occurred and potentially use this information to inform future management action.

Acknowledgements

Over the last two years while pursuing my Master of Science degree, I have learned that the scientific method rewards the individual who thinks deeply about the relationships around us. I am forever grateful for the significant contributions that my committee has made over the last two years and for continually pushing me to think deeper about my research. My advisor, Dr. Kennedy, has steadfastly provided guidance on navigating the complex process that is studying southern Appalachian forests. Dr. Bhuta and Dr. Thomas have contributed invaluable statistical help and provided direction on a variety of highly analytical approaches used in my research. The group of supportive graduate students in the Virginia Tech Environmental Tracking Lab have provided their individual expertise and helped form this project.

I would also like to thank the team at the USDA Forest Service, Coweeta Hydrologic Lab for their cooperation on providing the historical *in-situ* data used in this study. The support of Dr. Andrew Oishi and Dr. Peter Caldwell will not go unnoticed, in addition to the countless other Forest Service employees devoted to studying our unique southern Appalachian forests. Tyler Tran, previously an undergraduate researcher at Coweeta, was also instrumental in putting us in contact with individuals at Coweeta. We were also inspired by the work of Justin Braaten in combining multiple remote sensing archives.

I am also deeply grateful for my family, as their support for my academic pursuits has allowed me to dream big, break mental barriers, and continue to be ruthless about challenging myself.

Table of Contents

List of Figures

List of Tables

1. Introduction

1.1. Research Objectives

Invasive pests have substantially altered the species-rich eastern forests of the USA. Two important canopy species have suffered major declines related to invasive pests—eastern hemlock (*Tsuga canadensis* L. Carr.) and American chestnut (*Castanea dentata* (Marsh.) Borkh). One conifer, *T. canadensis*, has drastically declined in some areas since the introduction of the invasive hemlock woolly adelgid (*Adelges tsugae* Annand) in the 1950s (Krapfl, Holzmueller, and Jenkins 2011). Similarly, mature *C. dentata*, once the tallest tree in many eastern forests, was virtually eliminated from its overstory position by the invasive chestnut blight fungus (*Cryphonectria parasitica* (Murr.) Barr) by the 1950s (Woods and Shanks 1959).

Overstory die-offs of *C. dentata* and *T. canadensis* have allowed light to reach further into the canopies of many Appalachian forests. These overstory canopy gaps have allowed understory evergreen shrubs (UES) like rosebay rhododendron (*Rhododendron maximum* L.) and mountain laurel (*Kalmia latifolia* L.) to expand into areas where they were previously restricted (Woods and Shanks 1959; Krapfl, Holzmueller, and Jenkins 2011; Ford et al. 2012). The spatial expansion of *R. maximum* is well documented in some areas of the Appalachian Mountains (Dobbs and Parker 2004; Elliott and Vose 2012; Atkins, Epstein, and Welsch 2018). Dense thickets of *R. maximum* significantly alter forest structure and ecology by creating dense shading that inhibits the recruitment of canopy trees, reduces soil nutrients and moisture, and modifies soil seed banks (Clinton and Vose 1996; Cofer et al. 2018). Further expansion of *R. maximum* will continue to have substantial impacts on forest structure and function, making the monitoring of this phenomena important for Appalachian forest management. *K. latifolia*, having similar function and structure to *R. maximum*, might serve as an additional agent of change in southern

Appalachian forests. However, *K. latifolia* is relatively understudied when compared to the current body of literature on *R. maximum* expansion. Several studies have documented expansions of UES in the Southern Appalachians through comprehensive field-surveying techniques, though few have used remotely sensed data to document patterns in expansion across larger areas and for longer study periods (Krapfl, Holzmueller, and Jenkins 2011; Ford et al. 2012; Bolstad et al. 2018; Dharmadi, Elliott, and Miniat 2019).

One study, Atkins, Epstein, and Welsch (2018), examined *R. maximum* expansion along Weimar Run near Canaan Valley, West Virginia. While that study highlighted the utility of using remotely sensed data in studying *R. maximum*, the climate and geography of the study site were not necessarily representative of the central or Southern Appalachians. Our goal was to identify a study site indicative of the climate, topography, and ecology of the Southern Appalachians and document the expansions of both species of UES, *R. maximum* and *K. latifolia*, using remotely sensed data. Gaining a better understanding of the spatial and temporal patterns of UES expansion can help forest managers by pinpointing areas for management intervention. Documenting the possible expansion of UES in riparian areas might shed light on how its presence is impacting important riparian plant and animal species, which could be useful to stream ecologists concerned with *R. maximum*'s ability to alter the species diversity of allochthonous leaf litter inputs—an important source of energy in high-gradient headwater streams (Kominoski and Pringle 2009).

Our study involved the analysis of remotely sensed data to document characteristics of UES expansions in a well-known and highly studied model watershed of the southern Appalachian Mountains, the Coweeta Hydrologic Laboratory (CHL) in the Nantahala National Forest of North Carolina. Our main research objectives were 1) to leverage multi-decadal

archives of remotely sensed data to document potential UES expansions in the Coweeta watershed across the longest time window possible; and 2) to investigate the role of terrain position (elevation, aspect, slope, distance-from-stream) in the spatiotemporal expansion of UES.

1.2. Overstory Die-offs

The introduction of invasive species has dramatically altered forests in the eastern United States over the last century. *T. canadensis* and *C. dentata* were historically common overstory tree species in eastern forests but have been virtually extirpated from their native ranges due to the introduction of invasive pests. *T. canadensis* is especially vulnerable to the invasive insect *A. tsugae*, likely delivered to the United States from Japan on shipping materials in the 1950s. *A. tsugae* subsequently spread from Virginia to most of *T. canadensis*' native Appalachian range (Krapfl, Holzmueller, and Jenkins 2011). This study also documented that *A. tsugae* infection, although somewhat slow, results in heavy foliar losses and eventually the complete death of infected trees. *A. tsugae* infections cause significant decreases in the density (stems/ha) of overstory *T. canadensis* trees and without regard to local environmental variables like aspect, slope, and elevation (Krapfl, Holzmueller, and Jenkins 2011). *T. canadensis* overstory recruitment is threatened by *A. tsugae* infection, as understory hemlock individuals are documented to be especially vulnerable to infection (Krapfl, Holzmueller, and Jenkins 2011). Ford et al. (2012) documented that foliar losses in infected stands of *T. canadensis* were identical to the response seen in stands where trees were manually girdled (with 100% mortality). These results show that once *A. tsugae* infection occurs in a particular forest stand, the infection is virtually uncontrollable and limited to almost no area without proper management.

Similarly, *C. dentata* has also suffered similar wide-spread losses due to the introduction of an invasive species. The microscopic spores of *C. parasitica* were initially discovered in

1904 in New York City, New York, and were suspected to be brought from Asia on shipping materials (Woods and Shanks 1959). Before the introduction of *C. parasitica*, *C. dentata* was one of the largest and most common trees in eastern North America. Its original range spanned to areas east of the Mississippi River, from northern Florida to southern regions of eastern Canada (Woods and Shanks 1959). *C. dentata* was highly valued for the quality of timber and nuts it produced. Once *C. parasitica* was introduced, it spread rapidly throughout *C. dentata*'s native range at a rate of 30–40 km/year (Evans and Finkral 2010). *C. parasitica* fungal spores germinate on the pores of *C. dentata*, eventually leading to a girdling of infected trees (Woods and Shanks 1959). Although stump sprouts continue to grow and die without reproductive success, *C. dentata* has been functionally removed from its role as an ecologically important overstory tree species (Evans and Finkral 2010).

1.3. Life Histories of R. maximum and K. latifolia

R. maximum (family Ericaceae) is a common understory evergreen component in forests of eastern North America, from northern Georgia to Nova Scotia (NCSU Extension 2021). *R. maximum* produces long, waxy oblanceolate leaves that can remain on plants for up to eight years (Anderson 2008). These leaves are hardy and leathery (sclerophyllous) and therefore do not degrade quickly (Kominoski and Pringle 2009). Most individuals grow 10–20 ft tall, with some larger individuals recorded at over 40 ft. *R. maximum* can tolerate a variety of environments but proliferates in mesic areas relatively high in soil moisture, such as lower elevations, north-facing slopes, and coves in the Southern Appalachians (Anderson 2008; Bolstad et al. 2018).

K. latifolia, another common ericaceous shrub in forests of the Southern Appalachians,

occupies an extensive geographical range with records from Alabama to Quebec, Canada (League 2005). In contrast to *R. maximum*, *K. latifolia* inhabits relatively xeric sites like ridgetops and south-facing slopes, often as an associate to some pine and oak species (Monk, McGinty, and Day 1985). While normal growth rates for *R. maximum* and *K. latifolia* are relatively slow compared to other species of understory vegetation, *K. latifolia* grows vigorously after intense fires at a rate up to 4.8 in/year in height (League 2005; Horton et al. 2009).

1.4. Formation of Understory Evergreen Shrub Thickets

R. maximum thickets are commonplace in the Southern Appalachians and have important ecological roles in regulating forest understory processes. *R. maximum* can alter vegetation successional trends by limiting nutrients in soils, regulating light availability, modifying soil seed banks, and covering the ground in dense leaf litter (Krapfl, Holzmueller, and Jenkins 2011; Ford et al. 2012). While *T. canadensis* exhibits a higher rate of recruitment compared to other species of overstory trees when growing in *R. maximum* thickets, *A. tsugae* can severely limit *T. canadensis* recruitment and stands can quickly transition to dense *R. maximum* thickets (Krapfl, Holzmueller, and Jenkins 2011). *K. latifolia* can also form dense thickets induced by the presence of overstory canopy gaps which may occur due to canopy die-offs, logging, or fire (Clinton, Boring, and Swank 1994). While some studies have described *R. maximum* and *K. latifolia* thicket formation, few have evaluated the spread of these shrubs on the landscape-scale in the southern Appalachian Mountains.

1.5. R. maximum's Suppression of Overstory Tree Recruitment

An extensive body of literature documents the influence of *R. maximum* thickets on forest successional trends. *R. maximum*'s unique life history characteristics and physiological traits tend to inhibit the germination and growth of many ecologically and economically important

overstory trees species, especially through dense shading of forest floors. This shading blocks as much as 95% of available light, preventing overstory tree seedling germination (Ford et al. 2012). *R. maximum* also alters overstory successional trends through production of a dense layer of leaf litter that resides below shrubs. *R. maximum* does not defoliate before the winter months, and instead frequently drops leaves throughout the year that can form thick layers of peat up to 10 cm in depth (Lei et al. 2002). This litter layer inhibits normal seedling germination by reducing soil moisture content and by forming a physical barrier that blocks the emergence of overstory tree seedlings (Anderson 2008).

R. maximum also inhibits canopy tree seedling germination by modifying soil seed banks. Cofer et al. (2018) found that areas with dense thickets of *R. maximum* harbored a lower average seed bank richness and contained nearly twice the amount of *R. maximum* seeds when compared to seed bank samples from hardwood forests absent of *R. maximum*. This skewing of seed banks in locations with *R. maximum* thickets can lead to an increase in competition between overstory and shrub seedlings, while also severely suppressing forb-seed dispersal and diversity (Cofer et al. 2018). Overall, *R. maximum* expansion presents a 'multi-pronged' threat to overstory tree species and a unique management challenge that many forestry agencies may find alarming.

1.6. R. maximum in Riparian Areas

Several studies have documented *R. maximum*'s ability to alter the ecology in riparian areas. Baker and Van Lear (1998) studied the effect of *R. maximum* as an ecosystem modifier in near-stream environments, finding that areas high in *R. maximum* basal area and thicket densities led to a 77% decrease in riparian vegetation species richness when compared to areas with less *R. maximum*. The diversity of aquatic biota in headwater streams is also affected by the presence of *R. maximum*. The thick, hardy leaves of *R. maximum* are less palatable to some aquatic

fungus, bacteria, and benthic macroinvertebrate species. In a study of the breakdown of different species of leaf litter in headwater streams of western North Carolina, Kominoski and Pringle (2009) documented that *R. maximum* leaves decayed at a slower rate than leaves from other species of common trees like tulip poplar (*Liriodendron tulipifera* L.), red maple (*Acer rubrum* L.), and chestnut oak (*Quercus prinus* L.). Lower rates of breakdown in *R. maximum* leaves were linked to a lower diversity of common stream biota, like periphyton (aquatic bacteria) and benthic macroinvertebrates (Kominoski and Pringle 2009). The growing body of literature on *R. maximum* in riparian areas provides additional evidence of this species' ability to change terrestrial and aquatic environments and point to the importance of documenting UES on a landscape scale.

1.7. Remote Sensing of UES Expansion

Most studies of *R. maximum* expansion in response to overstory die-offs rely on standard field-based surveys, though a few studies have employed remote sensing techniques. Atkins, Epstein, and Welsch (2018) analyzed Landsat-5 Thematic Mapper (TM) imagery acquired from 1986–2011 for the Weimer Run watershed in West Virginia. Imagery, and the greenness indices that were subsequently extracted, were evaluated in snow-free scenes acquired during leaf-off time periods to allow for sufficient viewing of understory evergreen shrubs. The study documented an increase in winter greenness, especially near streams and on southerly-oriented slopes, and results were verified through field surveys to be caused by an expansion of *R. maximum* (Atkins, Epstein, and Welsch 2018). While Atkins, Epstein, and Welsch (2018) highlighted the importance of using remote sensing techniques to document *R. maximum* expansion, the study area was not entire representative of watersheds commonly found in the Southern Appalachians.

Only two studies have documented the proliferation of UES in the Coweeta Creek basin using remotely sensed data. Dobbs and Parker (2004) used digitized-film aerial photography from two discreet scenes, 1976 and 1993, and documented a strong relationship between topographic setting and UES expansion. Secondly, Bolstad et al. (2018) utilized five years (2005–2010) of optical and lidar data and related decreases in overstory biomass due to the presence of UES.

Overall, the use of remote sensing platforms in monitoring UES expansion in the Southern Appalachians has the potential to monitor the movement of these shrub species on a landscape-scale and over long time periods without the use of arduous field surveying techniques. However, there is a limited body of literature on using remote sensing platforms to monitor the expansion of UES. Our study aims to fill this literature gap by documenting the multi-decadal spread of UES in the Coweeta watershed.

2. Methods

2.1. Study Area

The Coweeta Hydrologic Laboratory (CHL) is a USDA Forest Service research station that has been operated since 1934 (Miniat et al. 2021). Located near Otto, North Carolina, this experimental forest contains a small, high-gradient watershed that is generally representative of watersheds in the Nantahala Mountains of western North Carolina (Figure 1). Like many forests in the southern Appalachian Mountains, the climate at CHL consists of frequent low-intensity rainstorms that contribute to its average yearly rainfall of 181 cm (Boring and Swank 1984; Swift, Cunningham, and Douglass 1988). Research originating from CHL often involves documenting local hydrologic, atmospheric, and vegetation patterns and related long-term ecological changes. Data from past and current studies conducted at CHL are routinely published

and often available for public use. Conducting this study at CHL offered a unique opportunity to observe long-term changes in UES using a combination of remotely sensed imagery and publicly available field data in a model southern Appalachian watershed.

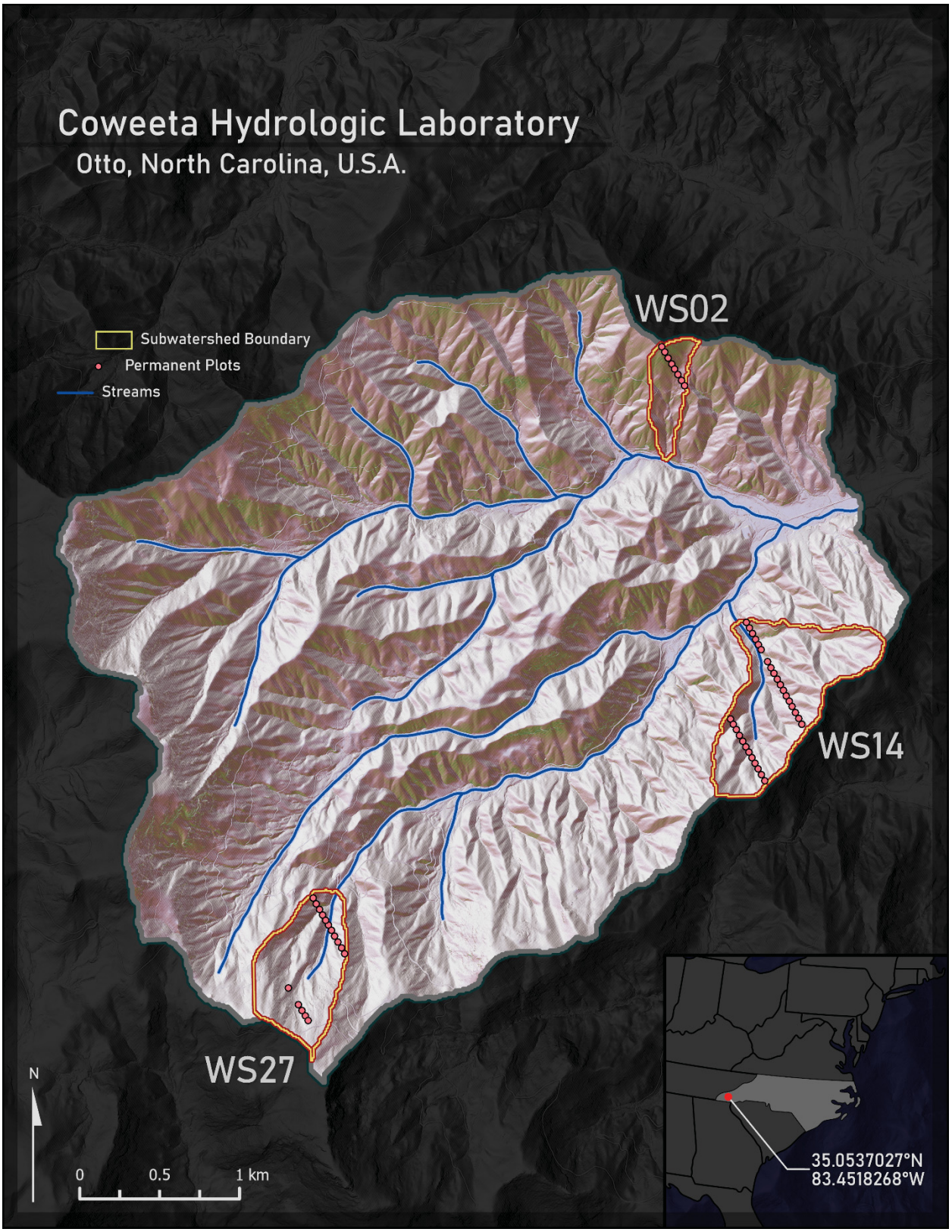

Figure 1. The Coweeta Hydrologic Laboratory. Reference watersheds (2, 14, 27) are outlined. Permanent plots are symbolized as red dots.

2.2. Harmonization of Landsat Imagery

One of our initial goals identified early in our research was to observe the expansion of UES throughout a large temporal window. The Landsat program is nearing 50 years of global-scale imagery acquisition and offers a large catalogue of multispectral products (Wulder et al. 2019). We retrieved Landsat imagery within the cloud-computing platform, Google Earth Engine. The powerful Earth Engine application programming interface offers users the ability to efficiently query large, inter-decadal archives of remote sensing products (Gorelick et al. 2017). Using Earth Engine allowed us to quickly filter hundreds of images from multiple sensors based on a variety of scene characteristics. Our data sets included collection 1, tier 1 surface reflectance imagery from Landsat-5 (Thematic Mapper; TM), Landsat-7 (Enhanced Thematic Mapper Plus; ETM+), and Landsat-8 (Operational Land Imager; OLI).

Similar to a method employed by Vogeler et al. (2018), we accounted for inter-sensor differences by applying harmonization coefficients to Landsat-5 TM and Landsat-7 ETM+ datasets for adequate comparisons with Landsat-8 OLI data (Table 1; Roy et al. 2016). Roy et al. (2016) developed ordinary least squares (OLS) regression transform-functions, including slope and intercept harmonization coefficients, by evaluating near-date swath edge overlaps between Landsat 7 and 8 data. While these harmonization coefficients were developed using only Landsat 7 and 8, we applied the same transform functions to Landsat-5 (now decommissioned) as this sensor occupied the same sun-synchronous 98.2° orbit as the currently operational Landsat-8 (Roy et al. 2016). Furthermore, the spectral ranges of bands 1–4 were virtually identical for Landsat 5 and 7 (USGS 2022; Table 1). To evaluate the efficacy of implementing harmonization coefficients, we created an identical dataset containing un-harmonized imagery to compare with harmonized data for imagery collected over CHL.

While Landsat-7 imagery provided data for the two years for which we lack Landsat 5 or 8 data (2012, 2013), Landsat-7 data were closely scrutinized due to the sensor's scan line corrector (SLC) malfunction that took place during May 2003 (Roy et al. 2016). SLC-off Landsat-7 data sometimes include gaps in usable spectral data in a given image.

2.3. Masking and Filtering Landsat Imagery

Reid et al. (2016) documented green chromatic coordinate (GCC) as a metric for phenological change because of the index's ability to quantify the amount of green light relative to blue and red light. In identifying the ideal leaf-off period of time for this study, we used GCC data (PhenoCam) recorded at CHL (Seyednasrollah et al. 2019). We noted relatively little change in GCC at CHL during December 1–March 16 for all years from 2016–2022. Landsat 5, 7, and 8 imagery were queried in Google Earth Engine for December 1–March 16 for 1985–2021 to allow for adequate leaf-off observations of UES without influences from late fall/early spring phenological changes.

Pixel quality assessment (QA) bands (i.e., CFmask bands) for all un-harmonized/harmonized Landsat imagery were used to mask areas high in cloud cover and cloud shadow to allow for adequate atmospheric opacity (Zhu, Wang, and Woodcock 2015).
We masked areas identified as containing snow in the pixel QA information to prevent the skewing of spectral information caused by the presence of snow in a scene. Including years that overlapped between sensors, these procedures produced a combined dataset of 339 Landsat images. After our masking and filtering procedures were complete, we generated a composite image for each of the 36 years in our study period. Imagery temporal aggregation methods (i.e., mean and median) have been shown to be as accurate as time series analyses, but with the added incentive of reducing data volume (Phan, Kuch, and Lehnert 2020). Rather than producing a time

series of winter NDVI for each year, we aggregated the average of six Landsat images per sensor for each year by reducing each year's image collection to its median pixel value (Phan, Kuch, and Lehnert 2020).

2.4. NDVI

Spectral data collected by sensors in the red (~0.66 μm) and near-infrared (NIR; ~0.85 μm) portions can be used to quantify the amount of photosynthetic plant biomass (Tucker 1979). One such index, the normalized difference vegetation index (NDVI), utilizes red and NIR light to quantify the presence and health of vegetation (greenness). We employed a similar method used by Atkins, Epstein, and Welsch (2018) by observing yearly changes in winter NDVI to track expansions of UES. We calculated NDVI using the following formula:

$$\text{NDVI} = \frac{\text{NIR} - \text{Red}}{\text{NIR} + \text{Red}}$$

2.5. Generating Terrain Data Layers

We compared changes in NDVI to common terrain parameters in efforts to better understand the spread of UES over the last 36 years. We used data from the Shuttle Radar Topography Mission (SRTM), which provided a vast library of virtually global-scale digital elevation models (DEMs) often used in terrain analysis research (Farr et al. 2007). We prepared layers for elevation, slope, and aspect using data from one arc-second (30 m) SRTM data and then generated a distance-from-stream layer in ArcGIS Pro (2.7.2) by calculating the Euclidean distance for each 30m cell to the closest stream within CHL.

Table 1. Area, elevation, slope, aspect, and number of permanent plots for CHL and subwatersheds.

	CHL (entire watershed)	**WS02**	**WS14**	**WS27**
Area (km^2)	16.67	0.14	0.63	0.40
Mean Elevation (m)	1004.66	866.90	891.66	1274.18
Mean Slope (degrees)	19.91	21.35	17.28	22.70
Mean Aspect	SSE	SSE	WSW	SE
# of Permanent Plots	54	8	30	16

Table 2. Per-band OLS slope/intercept harmonization coefficients are provided (Roy et al. 2016). Bands listed were used in this analysis, with band designations and subsequent spectral ranges (µm) included (USGS 2022). Date ranges of imagery included in this study are provided for each sensor.

	Landsat-5 TM (1986–2011)	**Landsat-7 ETM+** (2000–2021)	**Landsat-8 OLI** (2014–2021)	**Slope (ETM+ to OLI)**	**Intercept (ETM+ to OLI)**
Blue (30 m) **(µm)**	Band 1 (0.45–0.52)	Band 1 (0.45–0.52)	Band 2 (0.45–0.51)	0.8474	0.0003
Green (30 m) **(µm)**	Band 2 (0.52–0.60)	Band 2 (0.52–0.60)	Band 3 (0.53–0.59)	0.8483	0.0088
Red (30 m) **(µm)**	Band 3 (0.63–0.69)	Band 3 (0.63–0.69)	Band 4 (0.64–0.67)	0.9047	0.0061
Near infrared (30 m) **(µm)**	Band 4 (0.76–0.90)	Band 4 (0.77–0.90)	Band 5 (0.85–0.88)	0.8462	0.0412

2.6. Forest Inventory Data from Permanent Plots at CHL

In preparation for our analysis of possible expansions of UES at CHL, we requested and received *in-situ* forestry inventory data from CHL staff for three reference (control) subwatersheds (Figure 1). These data were adapted from Caldwell et al. (2016) and included information for all three subwatersheds with sampling events in 1970, 1990, and 2010. Two of the reference subwatersheds, WS02 and WS14, have remained unmanaged since 1927, and the third, WS27, since sometime around the creation of CHL in 1934 (Swank and Vose 1997). Information shared included diameter-at-breast-height (dbh), number of stems, and basal area of live trees/shrubs greater than 0.6 in (1.52 cm) in 54 permanent 20×40-meter plots arranged in approximately N-S (330°) transects (Caldwell et al. 2016). Measurements of basal area and stem density were included for both species of UES, *C. dentata*, *T. canadensis*, pitch pine (*Pinus rigida* Mill.), and white pine (*Pinus strobus* L.). Data from permanent plots were used to compare trends observed from satellite-borne multispectral platforms. In addition to observing a coincident change in UES and *T. canadensis* through time, we also aimed to observe possible changes between these species and others including *P. rigida*, *P. strobus*, and *C. dentata*.

3. Results

3.1. Inter-sensor Harmonization

We compared the magnitude of difference between harmonized and un-harmonized imagery acquired during the same years. Composite imagery generated for coinciding years, Landsat 5/7 (n = 22 years) and Landsat 7/8 (n = 8 years), followed similar trends (Figure 2). However, six of our 22 Landsat-7 composite images presented significant SLC-off errors (i.e., artifacts from voids and conspicuously higher NDVI in the shape of scan lines) when compared to imagery collected by other Landsat sensors for the same year (Figures 3 and 4). Therefore, we

prioritized imagery collected by sensors that do not present SLC-off errors (Landsat 5 and 8) and only used harmonized Landsat-7 imagery to fill the two-year gap in our dataset. The Landsat-7 scenes for 2012 and 2013 did not show artifacts from SLC-off errors (Figures 5 and 6). We observed a general increase in inter-sensor annual mean NDVI from 1986–2021 (Figure 7). Additionally, this plot included a non-parametric locally weighted line, or locally estimated scatterplot smoothing (loess), that preserved local changes (~5 years) in NDVI (Cleveland and Devlin 1988).

3.2. Terrain and Changes in NDVI

We observed dynamic changes in NDVI with respect to varying terrain parameters. Like our use of loess scatterplot smoothing lines, we chose to display plot lines using generalized additive models (GAM) that display multiple local regression lines to identify non-linear effects of terrain on NDVI (Hastie and Tibshirani 1987). GAMs performed better than loess smoothing at displaying changes in NDVI and terrain as this smoothing technique was able to handle this large dataset (n = 18,092) more efficiently.

Changes in NDVI from 1986–2021 were lowest (0.015) at elevations between 900–950 m (Figure 8). Elevations between 676–700 m and 1275–1300 m exhibited the greatest change in NDVI at 0.072 and 0.074, respectively (Figure 8). Slopes of 12°–14° showed the lowest change in NDVI (0.023), while steeper slopes of 33°–35° generated the highest change (0.060) (Figure 9). Northwest-facing aspects produced the lowest change in NDVI (0.012), while south-facing aspects yielded the highest change (0.057) (Figure 10). Changes in NDVI with respect to distance-from-stream were relatively static. The lowest change occurred at the minimum distance, 0–90 m (0.022), and the greatest change at the maximum distance, 600–800 m (0.043) (Figure 11).

3.3. NDVI and Forest Inventory Data for Subwatersheds

We included all values for basal area and stem density for all evergreen shrub and tree species (*K. latifolia*, *R. maximum*, *P. rigida*, *P. strobus*, *T. canadensis*) and one deciduous species, *C. dentata*. *P. rigid*a and *P. strobus* were included to examine their potential roles in winter greenness. In order to compare values for basal area ($m^2 \cdot hectare^{-1}$) and stem density ($stems \cdot hectare^{-1}$) between subwatersheds, we divided values for basal area and stem density by the total number of permanent plots per subwatershed (calculated as $m^2 \cdot hectare^{-1} \cdot plot^{-1}$ and $stems \cdot hectare^{-1} \cdot plot^{-1}$, respectively).

The field data for WS02 showed a decrease in basal area and stem density for *T. canadensis* and simultaneous increases in both UES after 1990 (Figure 12). NDVI remained relatively constant during 1970–1990 but increased rapidly soon thereafter. Basal area of UES increased in WS14 from 1970–2010 while *T. canadensis* increased before 1990 and decreased thereafter (Figure 13). Conversely, stem density in WS14 decreased for all species from 1970–2010. NDVI for WS14 slowly increased between 1986–2009 but increased dramatically after 2010. Lastly, WS27 showed substantial increases for basal area and stem density for UES between 1990–2010, with *R. maximum* showing a greater increase compared to *K. latifolia* (Figure 14). Similar to WS02 and WS14, field data for WS27 also showed a noticeable decrease in *T. canadensis* from 1990–2010. NDVI for WS27 decreased from 1986–2010, then increased until 2021.

Not surprisingly, *C. dentata* was almost absent from the field data representing all three subwatersheds as recruitment had been severely suppressed by the invasive blight before the first sampling year (1970). *P. rigida* and *P. strobus* were not abundant in WS02 and WS27 and we thus assumed them to have little effect on NDVI during our study period (Figures 12 and 14).

When compared to other tree species included in the field data, *P. rigida* was moderately abundant in WS14 in 1970 but soon after declined precipitously until 2010 (Figure 13).

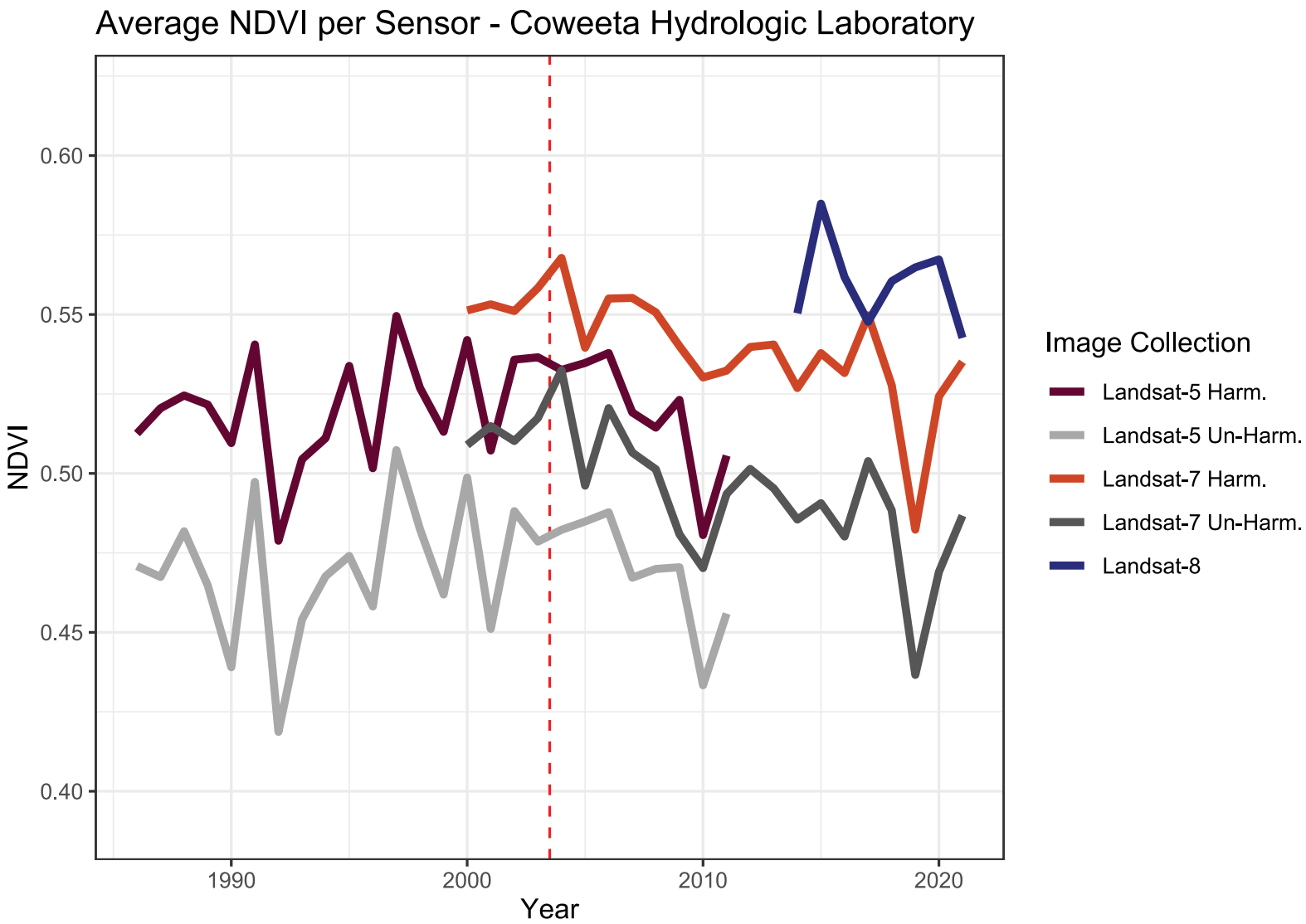

Figure 2. Average NDVI each year for each sensor (harmonized and un-harmonized). The Landsat-7 SLC-off malfunction occurred on May 31, 2003 (red dashed line).

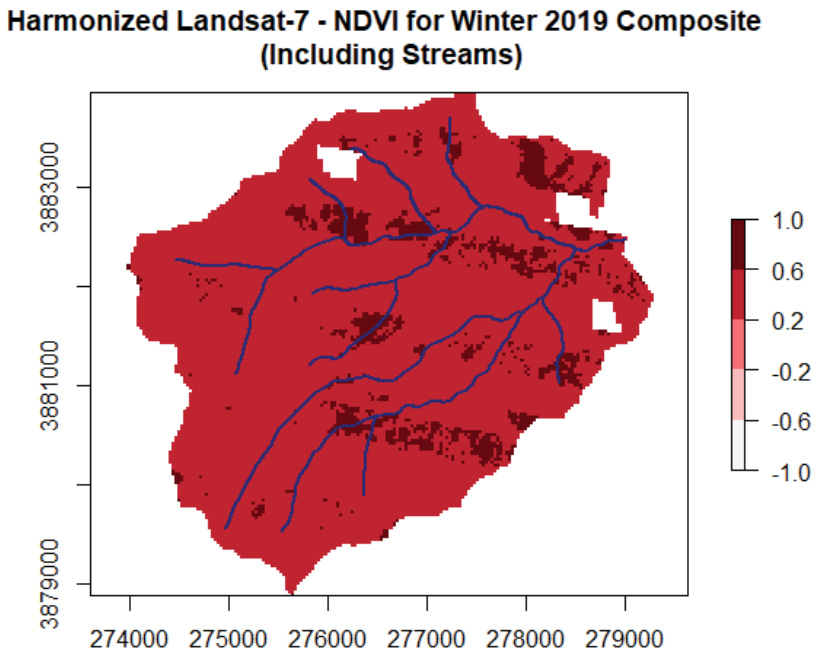

Figure 3. Map of harmonized Landsat-7 derived 2019 winter NDVI for CHL. Artifacts from SLC-off scanlines are indicated by parallel lines of higher NDVI.

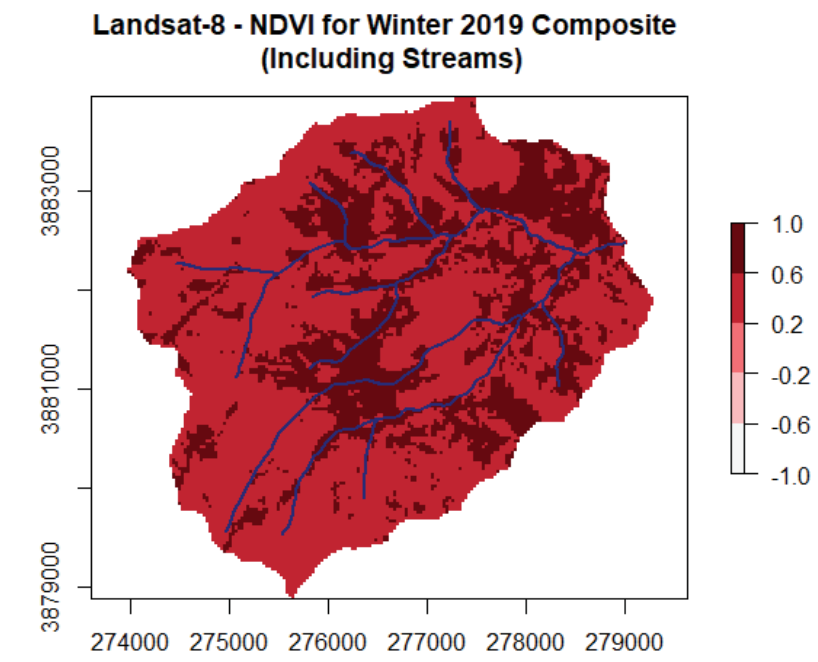

Figure 4. Map of Landsat-8 derived 2019 winter NDVI for CHL.

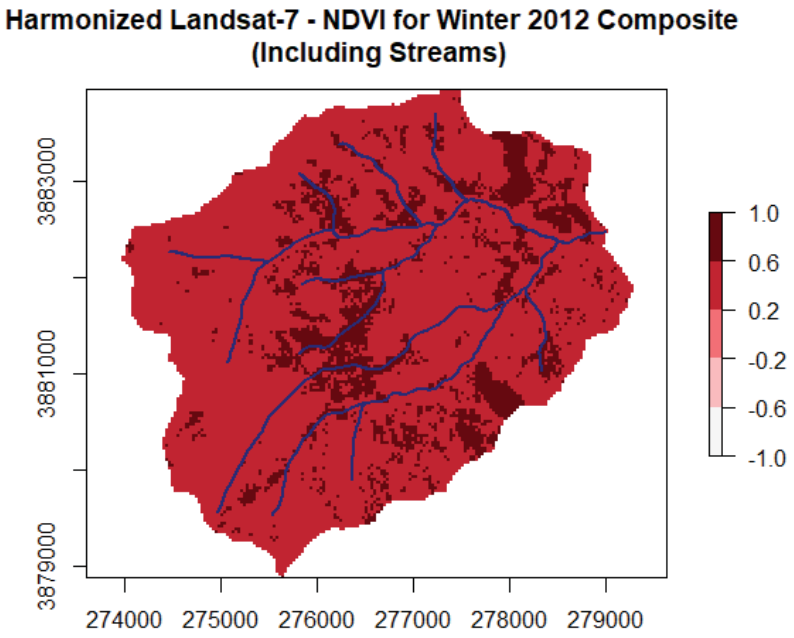

Figure 5. Map of harmonized Landsat-7 derived 2012 winter NDVI for CHL. These data were used to fill the gap in data between Landsat 5 and 8.

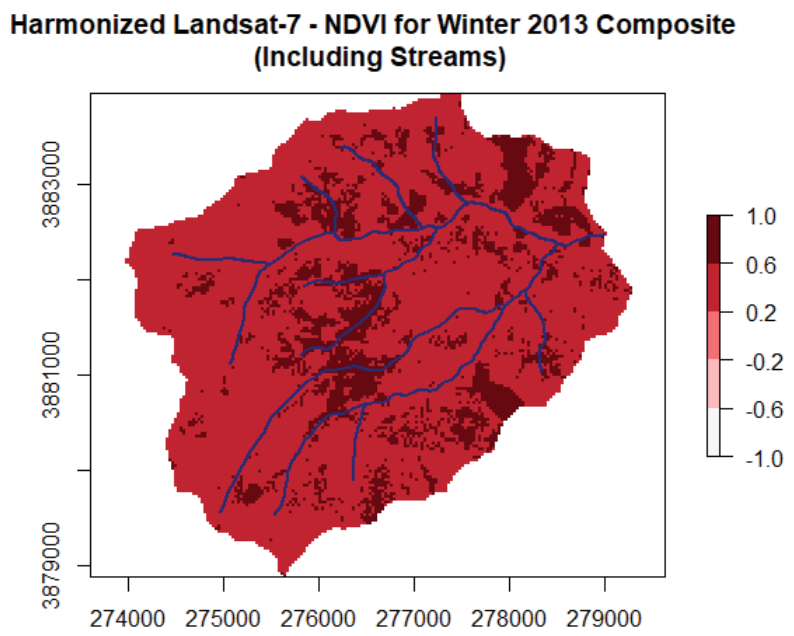

Figure 6. Map of harmonized Landsat-7 derived 2013 winter NDVI for CHL. These data were used to fill the gap in data between Landsat 5 and 8.

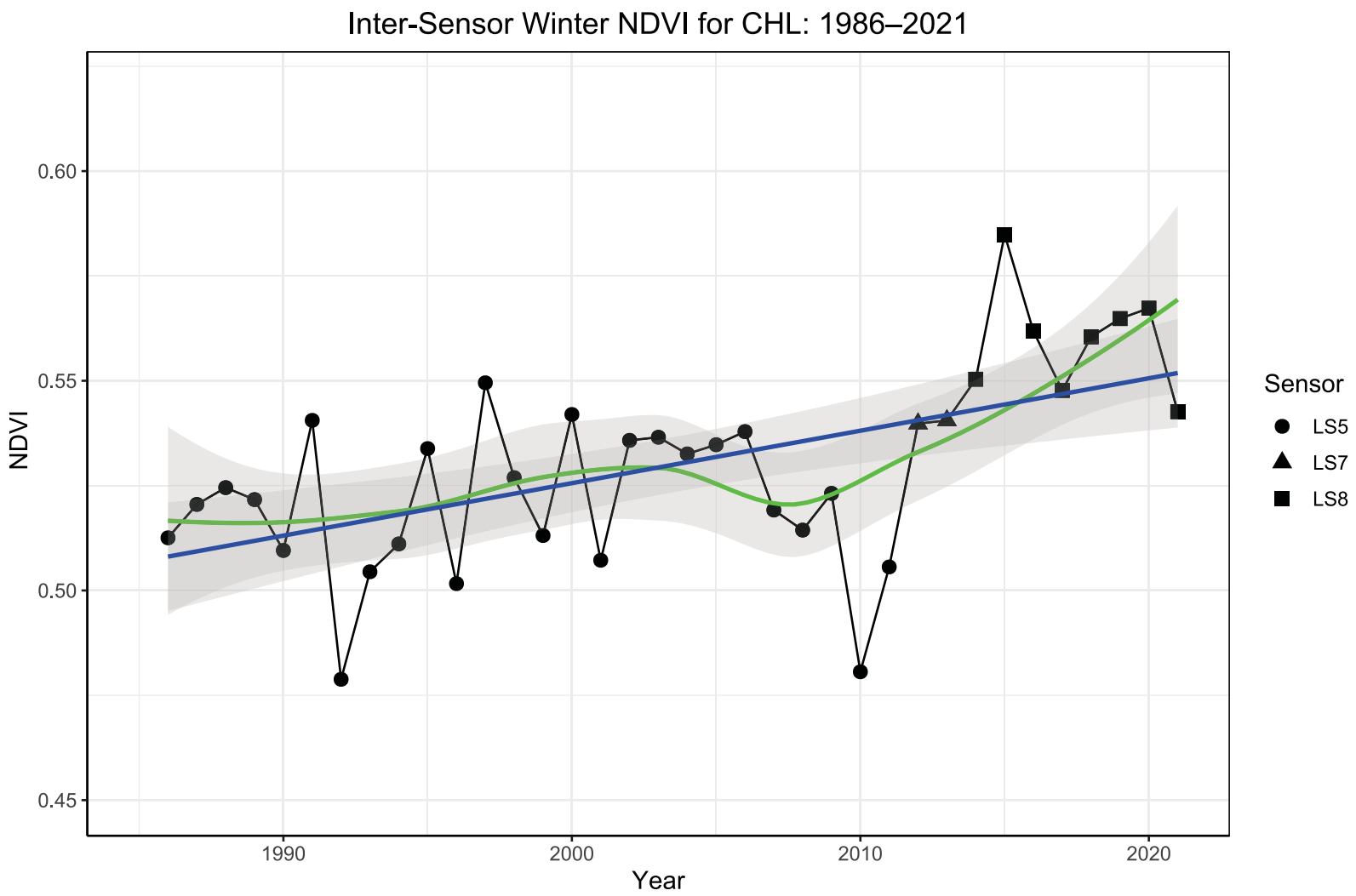

Figure 7. Average winter NDVI for 1986–2021 for the entire CHL watershed. Harmonized Landsat 5 and 7 were compiled with Landsat-8. NDVI was designated by sensor. The loess smoothing (green) line shows a general increase in winter greenness for CHL.

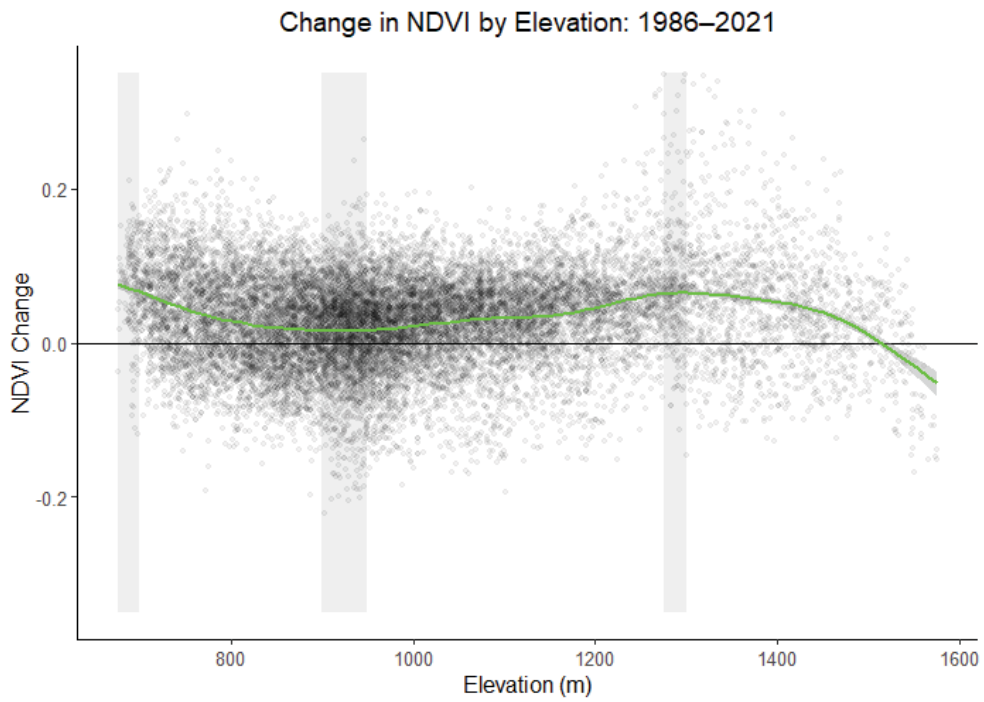

Figure 8. Change in NDVI (1986–2021) by elevation for the entire CHL watershed. Areas of relatively high/low NDVI change are shaded.

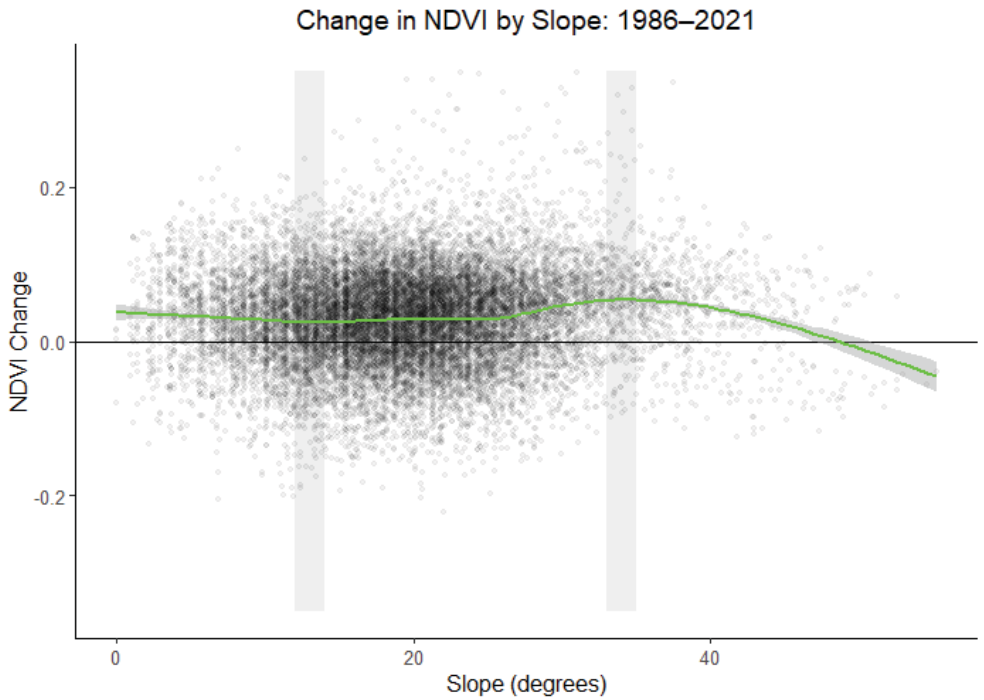

Figure 9. Change in NDVI (1986–2021) by slope for the entire CHL watershed. Areas of relatively high/low NDVI change are shaded.

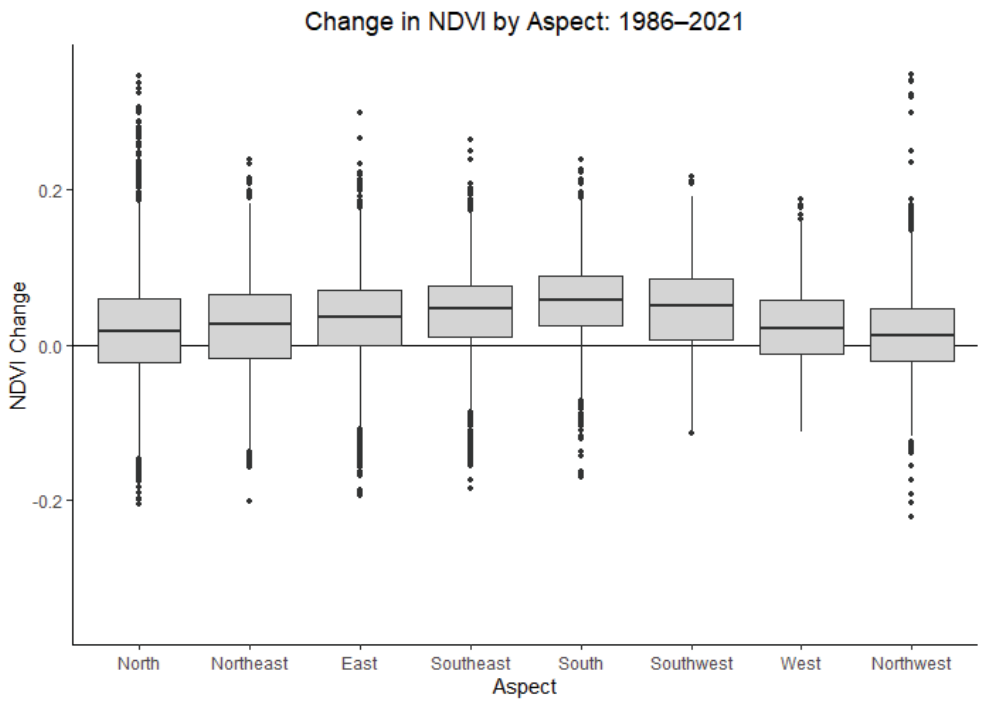

Figure 10. Change in NDVI (1986–2021) by aspect for the entire CHL watershed.

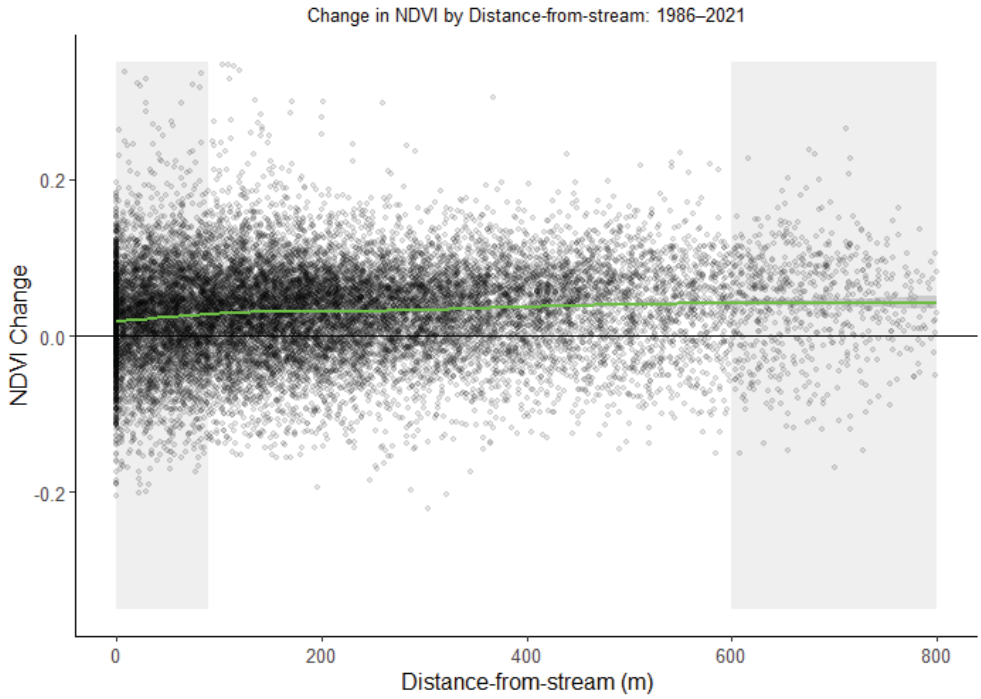

Figure 11. Change in NDVI (1986–2021) by distance-from-stream for the entire CHL watershed. Areas of relatively high/low NDVI change are shaded.

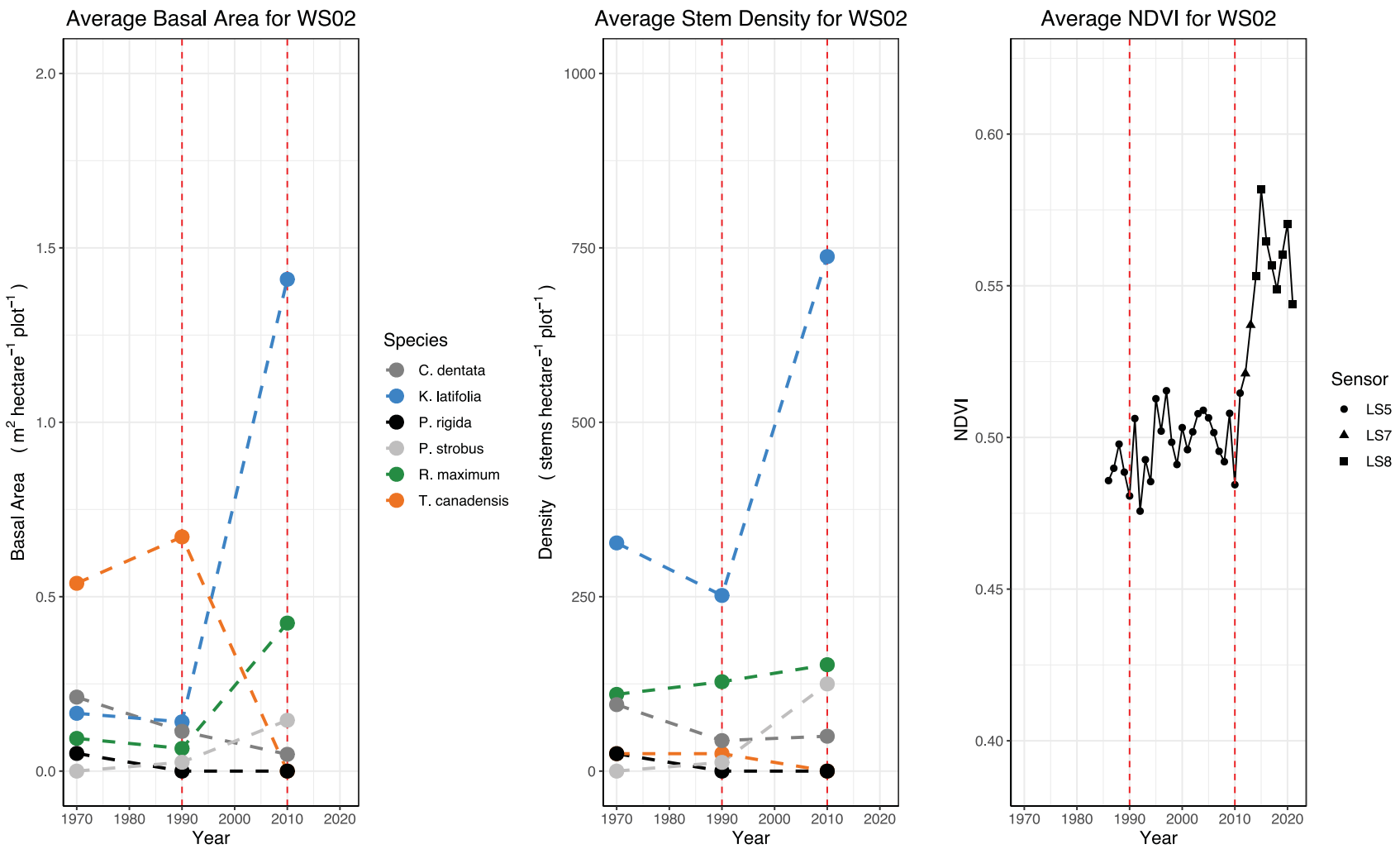

Figure 12. Comparison of average basal area/stems per plot and NDVI for watershed 2 (WS02). Red dashed lines represent overlaps in *in-situ* measurements and NDVI.

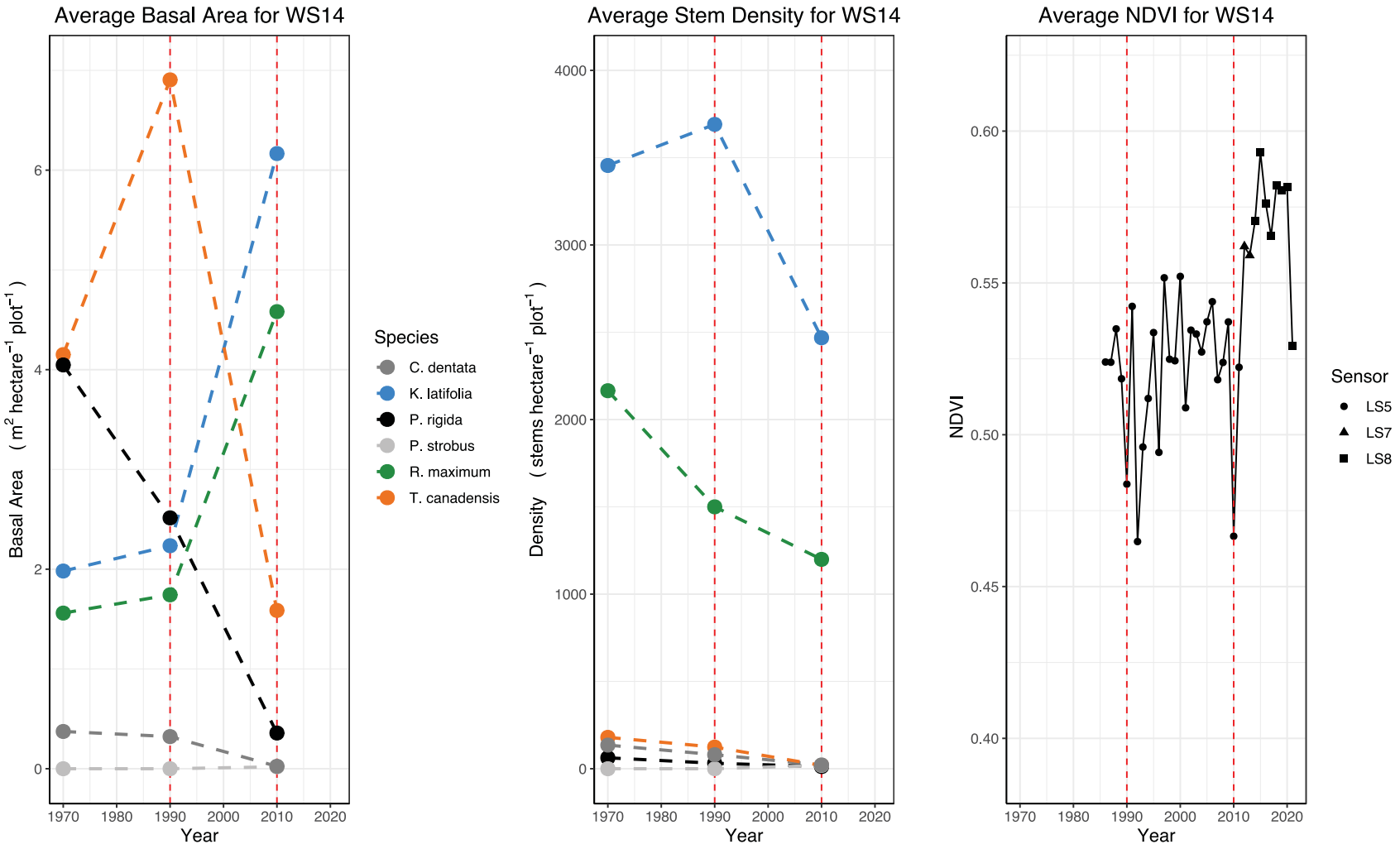

Figure 13. Comparison of average basal area/stems per plot and NDVI for watershed 14 (WS14). Red dashed lines represent overlaps in *in-situ* measurements and NDVI.

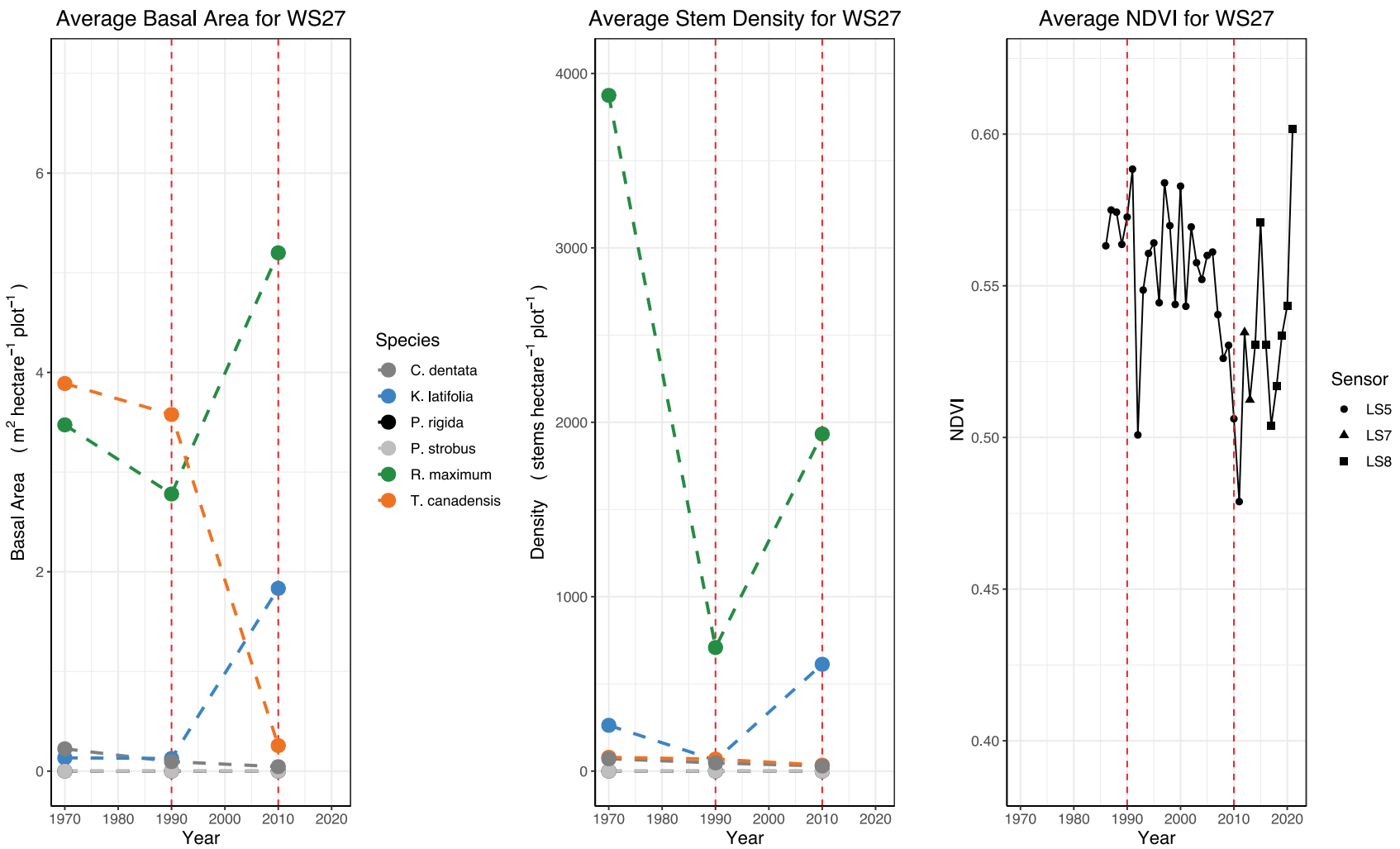

Figure 14. Comparison of average basal area/stems per plot and NDVI for watershed 27 (WS27). Red dashed lines represent overlaps in *in-situ* measurements and NDVI.

4. Discussion

4.1. Observing Inter-decadal Changes in UES

Previous studies using remotely sensed data to observe changes in UES were limited by shorter study periods (Dobbs and Parker 2004; Bolstad et al. 2018; Atkins, Epstein, and Welsch 2018). While increasing the timeframe for studying UES can seem easy at first, querying imagery from multiple decades and sensors is computationally-taxing. We used Landsat imagery from multiple sensors within the powerful cloud-computing platform, Google Earth Engine, to support a multi-decadal analysis (1986–2021) of UES expansion at CHL. In order to have the most accurate comparisons between three Landsat sensors, we applied per-band harmonization coefficients listed in Roy et al. (2016). Including years that overlapped between sensors, we generated a combined dataset of 339 Landsat images. Generating separate un-harmonized image collections for all Landsat sensors allowed us to observe the role that harmonization coefficients play in attenuating differences inherent to combining imagery from multiple sensors (Figure 2).

We followed Phan, Kuch, and Lehnert (2020) in aggregating our average of six Landsat images per year per sensor by reducing each year's image collection to its median pixel value. The median temporal aggregation technique we used produced composite images that were generally free from voids. These composites allowed us to observe winter greenness virtually uninterrupted for every location (pixel) within CHL for 1986–2021. While the temporal aggregation technique we used still yielded some Landsat-7 SLC-off composites that showed scanlines (Figures 3 and 4), it also seemed to attenuate the severity of these artifacts in other composites (Figures 5 and 6). Overall, we demonstrated that aggregation techniques can be used to provide relatively high-quality composite images to supplement imagery during gaps in sensor

catalogues. The combination of imagery from multiple Landsat sensors offered us a unique opportunity to observe a general increase in winter greenness over 36 years at CHL (Figure 7).

4.2. Evidence of UES Releases – Old and New

We documented distinct increases in winter greenness with respect to landscape position in CHL for 1986–2021. Higher elevations (~1300 m; Figure 8), steeper slopes (~35°; Figure 9), and south-facing aspects (Figure 10) all showed the largest increases in winter greenness throughout our study period. These topographic settings tend to be xeric and are sites where *K. latifolia* often occurs, along with a canopy pine, *P. rigida* (Monk, McGinty, and Day 1985).

While previous studies like Woods and Shanks (1959) documented the simultaneous die-off of *C. dentata* and release of UES in the early 19th century, there is a growing body of literature focused on a similar release in *R. maximum* caused by die-offs of *T. canadensis* during the later portion of the century (Ford et al. 2012; Brantley et al. 2015; Dharmadi, Elliott, and Miniat 2019). At CHL, Elliott and Vose (2012) noted that the peak of *R. maximum* establishment occurred from 1931–1940 following the die-off of *C. dentata* in the 1930s. Given *R.* maximum's past expansion due to overstory die-offs, we expected winter greenness to similarly increase in mesic areas where *T. canadensis* was found historically (Dharmadi, Elliott, and Miniat 2019). Surprisingly, mesic sites, typically found in low-lying areas along streams away from ridgetops, experienced the lowest change in winter greenness for our study period. We documented little change in winter greenness at mid elevations (~925 m; Figure 8), on gradual slopes (~13°; Figure 9), oriented on northerly-facing aspects (Figure 10), and in areas close to streams (0–90 m; Figure 11). However, we did document an increase in winter greenness at the lowest elevations at CHL (~690 m; Figure 8), most likely related to *R. maximum* given that it is the appropriate habitat for this species. Winter greenness remained fairly static in most mesic areas during our

study period, likely representing a stall in *R. maximum* expansion during recent decades since the species has probably attained its maximum presence in many areas after the die-off of *C. dentata*. Overall, changes in winter greenness for the three subwatersheds are likely due to the documented increases in UES, with *K. latifolia* accounting for most of this expansion (Figures 12, 13, and 14). Yearly increases in greenness for our whole-watershed analyses (Figures 7, 8, 9, 10, and 11) are likely attributed to a combination of these releases as well. Given our lack of information on the complex spatial nature of management and disturbance history outside of the control subwatersheds, more field data would be necessary to extrapolate our interpretations of expansion to the whole of CHL.

Our comparison of NDVI and terrain variables allowed us to attribute the expansions to each of the two shrub species spatially by habitat types. Increases observed in *R. maximum* during our study period (Figures 12, 13, and 14) are likely due to the die-off of *T. canadensis* as this canopy tree often occupies similar mesic sites. Conversely, documented increases in *K. latifolia* in all subwatersheds (Figures 12, 13, and 14) are likely attributed to the loss of *P. rigida* from ridgetops as both species prefer xeric, rocky outcrops (Waterman et al. 1995; Williams 1998). The exclusion of fire from the three control subwatersheds is likely to be prohibiting the regeneration of fire-adapted species, like *P. rigida* (Williams 1998). Additionally, *P. rigida* densities in WS02 and WS14 (Figures 12 and 13) might be decreasing in response to the ever-present threat posed by the native southern pine beetle (*Dendroctonus frontalis* Zimmerman) (Heuss, D'Amato, and Dodds 2019). Even with *P. rigida* virtually absent in the subwatersheds after 2010, *K. latifolia* will likely continue to spread on ridgetop positions in unmanaged watersheds as this species suppresses overstory seedling establishment and limits overstory canopy height and biomass (Brose 2016; Bolstad et al. 2018).

Field data from permanent plots in each of the three subwatersheds show that both species of UES have made significant gains since the 1990s (Figures 12, 13, and 14). While we expected increases in *R. maximum* given the extensive literature documenting this phenomenon in Appalachian forests, *K. latifolia* exceeding *R. maximum* in measurements of both basal area and stem density in the three subwatersheds was particularly surprising.

4.3. Future Work

Continued research could employ data fusion techniques to document changes in the abundance and distribution of xerophytic evergreen shrub species, like *K. latifolia*. Such analyses are known to yield high classification accuracies by combining multiple remotes sensing products (Lamb, Tzortziou, and McDonald 2021). Future studies using fused datasets could leverage a combination of multispectral and InSAR radar data to classify areas at CHL with primarily *R. maximum* or *K. latifolia* understories. Future spaceborne imaging spectroscopy missions, like the German Aerospace Center's EnMAP, will eventually provide products with higher spectral resolutions and potentially species-level classification of UES on the landscape-scale (Guanter et al. 2015). Lastly, we aim to bolster the methods used in this study by adapting previous work that developed local harmonization coefficients for better spectral harmonization between Landsat sensors (Vogeler et al. 2018). Whichever methods future researchers deem appropriate for investigating changes in UES, these studies should account for *R. maximum* and *K. latifolia*'s typically slow growth rates (Horton et al. 2009). Studies with shorter time periods than ours might fail to document increases in evergreen shrubs and could be limited to using remotely sensed data that has been collected for multiple decades, like Landsat.

4.4. Conclusion

Leveraging harmonized inter-sensor data from multiple Landsat missions allowed us to document changes in evergreen vegetation over 36 years at the landscape-scale. Observing changes in winter greenness over multiple decades is especially important in the study of UES dynamics because of their slow growth. We generated high spatial (pixel) and temporal (yearly) resolution data that showed when and where evergreen shrubs were increasing and helped point to the drivers of change. We demonstrated that when properly harmonized, data from long-term remote sensing programs like Landsat can be used to document understory releases on a yearly basis and help to expand knowledge gained from field sampling events that may only occur at decadal intervals.

Our interpretation of winter greenness benefited from field data provided by CHL in addition to our analysis of the connection between terrain position and NDVI. The *in-situ* data collected from permanent plots in three unmanaged watersheds offered context to the previous loss of overstory trees that promoted the spread of UES. By comparing changes in winter greenness and terrain, we were able to confidently infer the expansions of UES at the species level. Our analysis of terrain variables and NDVI strongly suggests that increases in *K. latifolia* are primarily responsible for enhanced winter greenness for 1986–2021 across the watershed overall, but in particular at higher elevations, on steeper slopes, and on south-facing aspects.

Our results built on knowledge gained from previous research at CHL by documenting the proliferation of two important understory evergreen shrub species that are common throughout the Appalachian Mountains. These two species have strong influences on the future trajectory of southern Appalachian forest composition and structure. Our study has pointed to precise locations in which management efforts may be desirable.

References

Anderson, M. D. 2008. *Rhododendron maximum*. Fire effects information system, U.S. Department of Agriculture, Forest Service. https://www.fs.fed.us/database/feis/plants/shrub/rhomax/all.html (last accessed 10 November 2021).

Atkins, J. W., H. E. Epstein, and D. L. Welsch. 2018. Using Landsat imagery to map understory shrub expansion relative to landscape position in a mid-Appalachian watershed. *Ecosphere* 9(10).

Baker, T., and D. Van Lear. 1998. Relations between density of rhododendron thickets and diversity of riparian forests. *Forest Ecology and Management* 109(1).

Bolstad, P. V., K. J. Elliott, and C. F. Miniat. 2018. Forests, shrubs, and terrain: top-down and bottom-up controls on forest structure. *Ecosphere* 9(4).

Boring, L. R., and W. T. Swank. 1984. The role of black locust (*Robinia pseudo-scacia*) in forest succession. *Journal of Ecology* 72(3): 749–766.

Brantley, S. T., C. F. Miniat, K. J. Elliott, S. H. Laseter, and J. M. Vose. 2015. Changes to southern Appalachian water yield and stormflow after loss of a foundation species. *Ecohydrology* 8(3): 518–528.

Brose, P. H. 2016. Origin, development, and impact of mountain laurel thickets on the mixed-oak forests of the central Appalachian Mountains, USA. *Forest Ecology and Management* 374: 33–41.

Caldwell, P. V., C. F. Miniat, K. J. Elliott, W. T. Swank, S. T. Brantley, S. H. Laseter. 2016. Declining water yield from forested mountain watersheds in response to climate change and forest mesophication. Global Change Biology 22(9): 2997–3012.

Cleveland, W. S., and S. J. Devlin. 1988. Locally weighted regression: An approach to regression analysis by local fitting. *Journal of the American Statistical Association* 83(403): 596–610.

Clinton, B. D., L. R. Boring, W. T. Swank. 1994. Regeneration patterns in canopy gaps of mixed-oak forests of the southern Appalachians: Influences of topographic position and evergreen understory. *The American Midland Naturalist* 132(2): 308–319.

Clinton, B. D., and J. M. Vose. 1996. Effects of Rhododendron maximum L. on Acer rubrum L. seedling establishment. *Castanea* 61(1): 38–45.

Cofer, T. M., K. J. Elliott, J. K. Bush, and C. F. Miniat. 2018. Rhododendron maximum impacts seed bank composition and richness following Tsuga canadensis loss in riparian forests. *Ecosphere* 9(4).

Dharmadi, S. N., K. J. Elliott, and C. F. Miniat. 2019. Lack of forest tree seedling recruitment and enhanced tree and shrub growth characterizes post-Tsuga canadensis mortality forests in the southern Appalachians. *Forest Ecology and Management* 440: 122–130.

Dobbs, M. M., and A. J. Parker. 2004. Evergreen understory dynamics in Coweeta Forest, North Carolina. *Physical Geography* 25(6): 481–498.

Elliott, K. J., and J. M. Vose. 2012. Age and distribution of an evergreen clonal shrub in the Coweeta basin: *Rhododendron maximum* L. *Journal of the Torrey Botanical Society* 139(2): 149–166.

Evans, E., and A. Finkral. 2010. A new look at spread rates of exotic diseases in North American forests. *Forest Science* 56(5): 453–459.

Farr, T. G., P. A. Rosen, E. Caro, R. Crippen, R. Duren, S. Hensley, M. Kobrick, et al. 2007. The Shuttle Radar Topography Mission. *Reviews of Geophysics* 45(2).

Ford, C., K. J. Elliott, B. Clinton, B. Kloeppel, and J. Vose. 2012. Forest dynamics following eastern hemlock mortality in the southern Appalachians. *Oikos* 121(4): 523–536.

Gorelick, N., M. Hancher, M. Dixon, S. Ilyushchenko, D. Thau, and R. Moore. 2017. Google Earth Engine: Planetary-scale geospatial analysis for everyone. *Remote Sensing of Environment* 202: 18–27.

Guanter, L., H. Kaufmann, K. Segl, S. Foerster, C. Rogass, S. Chabrillat, T. Kuester, et al. 2015.The EnMAP spaceborne imaging spectroscopy mission for Earth observation. *Remote Sensing* 7(7): 8830–8857.

Hastie, T., and R. Tibshirani. 1987. Generalized additive models: Some applications. *Journal of the American Statistical Association* 82(398): 371–386.

Heuss, M., A. W. D'Amato, and K. J. Dodds. 2019. Northward expansion of southern pine beetle generates significant alterations of forest structure and composition of globally rare Pinus rigida forests. *Forest Ecology and Management* 434: 119–130.

Horton, J. L., B. D. Clinton, J. F. Walker, C. M. Beier, and E. T. Nilsen. 2009. Variation in soil and forest floor characteristics along gradients of ericaceous, evergreen shrub cover in the southern Appalachians. *Castanea* 74(4): 340–352.

Kominoski, J., and C. Pringle. 2009. Resource–Consumer Diversity: Testing the effects of leaf litter species diversity on stream macroinvertebrate communities. *Freshwater Biology* 54(7).

Krapfl, K., E. Holzmueller, and M. Jenkins. 2011. Early impacts of hemlock woolly adelgid in *Tsuga canadensis* forest communities of the southern Appalachian Mountains. *Journal of the Torrey Botanical Society* 138(1).

Lamb, B. T., M. A. Tzortziou, and K. C. McDonald. 2021. A fused radar-optical approach for mapping wetlands and deepwaters of the mid-Atlantic and Gulf Coast regions of the United States. Remote Sensing 13(13).

League, K. R. 2005. *Kalmia latifolia*. Fire effects information system, U.S. Department of Agriculture, Forest Service. https://www.fs.fed.us/database/feis/plants/shrub/kallat/all.html (last accessed 24 April 2022).

Lei, T., S. Semones, J. Walker, B. Clinton, and E. Nilsen. 2002. Effects of rhododendron maximum thickets on tree seed dispersal, seedling morphology, and survivorship. *International Journal of Plant Sciences* 163(6).

Miniat, C. F., A. C. Oishi, P. V. Bolstad, C. R. Jackson, N. Liu, J. P. Love, C. M. Pringle, et al. 2021. The Coweeta Hydrologic Laboratory and the Coweeta Long-Term Ecological Research Project. *Hydrologic Processes* 35(7).

Monk, C. D., D. T. McGinty, and F. P. Day. 1985. The ecological importance of Kalmia latifolia and Rhododendron maximum in the deciduous forest of the southern Appalachians. *Torrey Botanical Society* 112(2): 187–193.

NCSU Extension. 2021. *North Carolina Extension gardener plant toolbox: Rhododendron maximum*. https://plants.ces.ncsu.edu/plants/rhododendron-maximum/ (last accessed 15 November 2021).

Phan, T. N., V. Kuch, and L. W. Lehnert. 2020. Land cover classification using Google Earth Engine and Random Forest classifier—the role of image composition. *Remote Sensing* 12(15): 2411.

Reid, A. M., W. K. Chapman, C. E. Prescott, and W. Nijland. 2016. Using excess greenness and green chromatic coordinate colour indices from aerial images to assess lodgepole pine vigour, mortality and disease occurrence. *Forest Ecology and Management* 374: 146–153.

Roy, D. P., V. Kovalskyy, H. K. Zhang, E. F. Vermote, L. Yan, S. S. Kuman, and A. Egorov. 2016. Characterization of Landsat-7 to Landsat-8 reflective wavelength and normalized difference vegetation index continuity. *Remote Sensing of Environment* 185: 57–70.

Seyednasrollah, B., A. M. Young, K. Hufkens, T. Milliman, M. A. Fridel, S. Frolking, and A. D. Richardson. 2009. Tracking vegetation phenology across diverse biomes using version 2.0 of the PhenoCam dataset. *Scientific Data* 6(1): 1–11.

Swank, W. T., and J. M. Vose. 1997. Long-term nitrogen dynamics of Coweeta forested watersheds in the southeastern United States of America. *Global Biogeochemical Cycles* 11(4): 657–671.

Swift Jr., L. W., G. B. Cunningham, and J. E. Douglass. 1988. Climate and Hydrology. In *Forest hydrology and ecology at Coweeta*, ed. Swank, W. T., and D. A. Crossley Jr., 35–56. New York, New York, USA: Ecological Studies.

Tucker, C. J. 1979. Red and photographic infrared linear combinations for monitoring vegetation. *Remote Sensing of Environment* 8(2): 127–150.

USGS. 2022. *What are the band designations for the Landsat satellites*? Frequently asked questions. https://www.usgs.gov/faqs/what-are-band-designations-landsat-satellites#faq (last accessed 12 February 2022).

Vogeler, J. C., J. D. Braaten, R. A. Slesak, and M. J. Falkowski. 2018. Extracting the full value of the Landsat Archive: Inter-sensor harmonization for the mapping of minnesota forest canopy cover (1973–2015). *Remote Sensing of Environment* 209: 363–374.

Waterman, J. R., A. R. Gillespie, J. M. Vose, and W. T. Swank. 1995. The influence of mountain laurel on regeneration of pitch pine canopy gaps of the Coweeta Basin, North Carolina, U.S.A. *Canadian Journal of Forest Research* 25(11): 1756–1762.

Williams, C. E. 1998. History and status of Table Mountain pine–pitch pine forests of the southern Appalachian Mountains (USA). *Natural Areas Journal* 18(1): 81–90.

Woods, F. W., and R. E. Shanks. 1959. Natural replacement of chestnut by other species in the Great Smoky Mountains National Park." *Ecology* 40(3).

Wulder, M. A., T. R. Loveland, D. P. Roy, C. J. Crawford, J. G. Masek, C. E. Woodcock, R. G. Allen, et al. 2019. Current status of Landsat Program, science, and applications. *Remote Sensing of Environment* 225: 127–147.

Zhu, Z., S. Wang, C. Woodcock. 2015. Improvement and expansion of the Fmask algorithm: cloud, cloud shadow, and snow detection for landsats 4–7, 8, and Sentinel 2 images. *Remote Sensing of Environment* 159: 269–277.